THE EFFECT OF MICROSTRUCTURE AND PORE MORPHOLOGY ON MECHANICAL AND DYNAMIC PROPERTIES OF FERROUS P/M MATERIALS

Tina M. Cimino, Amie H. Graham, Thomas F. Murphy and Alan Lawley

ABSTRACT

The objective of this study was to quantify and understand the combined role of microstructure and pore characteristics on the transverse rupture strength (TRS), tensile properties and rotating bend fatigue response of conventional and ANCORDENSE processed FLN2-4405 premixes. To this end, the premixes were made with samples using fine (4µm) and coarse (50µm) nickel powder to promote differences in pore size and diffusion characteristics. Compacts were sintered in synthetic DA (75 v/o H_2 / 25 v/o N_2) at 2050°F (1120°C) or 2300°F (1260°C) to densities in the range of 6.8 g/cm³ - 7.2 g/cm³. Pore size and spacing, cumulative pore size and number of pores per unit area were determined by stereological analysis, and the crack path was monitored by means of optical microscopy. The static and dynamic properties of the materials made from the two premixes are interpreted in terms of the attendant microstructures and pore characteristics, as dictated by the premix type, sintering temperature and sintered density.

INTRODUCTION

A primary area of growth in the P/M industry is high performance applications, such as gears and sprockets. In order to continue penetration into these markets, understanding the key parameters that affect the fatigue endurance limit of P/M materials is becoming increasingly important. Previous studies have indicated that the fatigue endurance limit of P/M materials is not a fixed percentage of the ultimate tensile strength, but rather a complex relationship between the microstructural constituents and the pore structure.[1,2,3] However, the analysis has been complicated by the fact that these studies have included multiple alloy systems, which make it difficult to isolate the predominant factor.

Choosing the matrix for this study, which includes conventional and ANCORDENSE processed FLN2-4405 premixes with various nickel particle sizes, provided the ability to isolate the microstructure of the materials while modifying the porosity size and spacing.

A hybrid alloy with admixed nickel was chosen due to the following:

- It is widely used in high performance applications (gears, sprockets)
- Studies have shown the diffusion pattern of nickel is not typical of a fine particle sized additive
- Research indicates that nickel rich areas may play an important role in arresting fatigue crack propagation

As stated above, the present study, which is part of an ongoing program to evaluate dynamic properties of P/M materials at Hoeganaes, utilizes conventional and ANCORDENSE processed materials. ANCORDENSE is a patented material and compaction technology, which can achieve sintered densities in the range of 7.25 g/cm³ to 7.45 g/cm³ using conventional compaction pressures and sintering temperatures. The technology involves the use of a specifically engineered lubricant/binder system which acts to prevent segregation of the powder and increase lubrication of the die wall during compaction. The compaction process is carried out at an elevated temperature in the range of 265°F (130°C) to 310°F (155°C) with the lubricant/binder system designed to operate optimally in this range. One of the benefits of this process is the ability to produce high density parts with outstanding physical properties.[4] The fatigue properties were assessed in relationship to ultimate tensile strength and key stereological parameters. Optical microscopy was also conducted to evaluate the microstructures of the materials as well as the path of fatigue crack propagation.

MATERIALS AND PROCESSING

The compositions of the test materials that were analyzed in this study are detailed in Table I. The nickel used for this study was Novamet / Type 4SP ($d_{50} \sim 50$ µm) and Inco 123 ($d_{50} \sim 4$ µm). The graphite utilized in the study was Asbury 3203 HS and each mix included 0.75 w/o (weight percent) Lonza Acrawax.

Table I: Premix Compositions

Material	Processing Method	Base Powder	Graphite (w/o)	Nickel (w/o)	Nickel Particle Size (µm)
		Nominal Premix Additions			
A	Conventional	Ancorsteel 85 HP	0.5	2.0	$d_{50} \sim 50$
B	Conventional	Ancorsteel 85 HP	0.5	2.0	$d_{50} \sim 4$
C	ANCORDENSE	Ancorsteel 85 HP	0.5	2.0	$d_{50} \sim 50$
D	ANCORDENSE	Ancorsteel 85 HP	0.5	2.0	$d_{50} \sim 4$

To aid in data analysis, fatigue and tensile samples for materials A through D were compacted at various pressures to attain a minimum of two overlying density levels. Specimens were sintered in a 75 v/o H_2/ 25 v/o N_2 atmosphere for thirty minutes at temperatures of 2050°F (1120°C) and 2300°F (1260°C). Sintered chemistry values are shown in Table II below.

The dogbone specimens for tensile testing were utilized as compacted while the fatigue specimens were machined and ground to size, from a 0.45 inch x 0.45 inch x 3.5 inch (11.4 mm x 11.4 mm x 88.9 mm) nominal sized specimen, following the sintering operation.

After compaction and sintering, density was determined on samples by the immersion method outlined in MPIF Standard 42.[5] The as-sintered tensile properties were determined according to MPIF Standard 10 utilizing a 60,000 pound (266 kN) Tinius Olsen universal tensile tester.[5]

Table II: Sintered Chemistry Values

Material	Sintering Temperature °F / *°C*	Sintered Chemistry (w/o)	
		Nickel	Carbon
Mix A	2050 / *1120*	1.96	0.51
	2300 / *1260*	1.82	0.53
Mix B	2050 / *1120*	2.00	0.51
	2300 / *1260*	2.06	0.51
Mix C	2050 / *1120*	2.13	0.49
	2300 / *1260*	2.07	0.52
Mix D	2050 / *1120*	2.19	0.51
	2300 / *1260*	2.26	0.49

Rotating Bending Fatigue (RBF) Testing:

The fatigue properties were evaluated with rotating bending fatigue samples. Testing was performed on six randomly selected Fatigue Dynamics RBF-200 machines at a rotational speed of 8,000 rpm. These rotating bending machines are of the mechanical and non-resonant type and are an efficient means of inducing fatigue in a specimen of round cross section.[6] The dimensions of the specimens used for this analysis, along with the allowable dimensional tolerances, are shown in Figure 1. This is a widely used sample for metals as well as non-metals and has been accepted by several laboratories with only minor differences in dimensions.
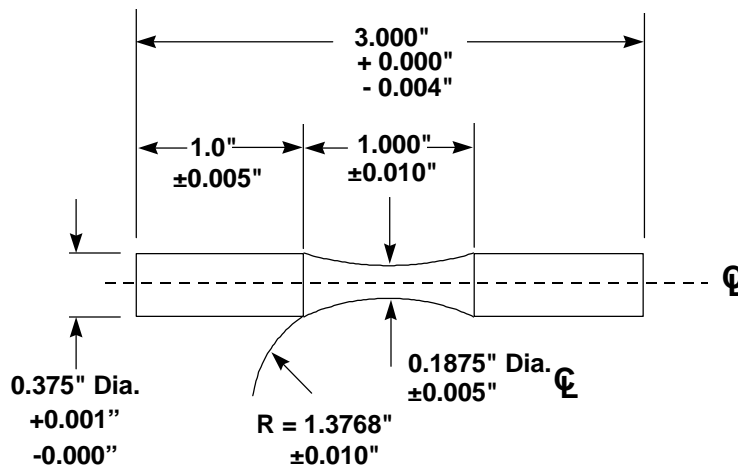
ALL DIAMETERS TO BE CONCENTRIC WITHIN 0.001"
SURFACE FINISH = 8 RMS (Polished Longitudinal)
Note: All Dimensions are in inches

Figure 1:   Dimensions of Rotating Bending Fatigue Specimen

Fatigue in a homogeneous material is usually a surface dependent phenomenon; the majority of fatigue failures originate at the surface.[7] During testing, one complete stress reversal occurs with each revolution of the specimen at the critical cross section. One of the drawbacks of the test is that due to the relatively small size of RBF test specimens, only a small volume of material is subjected to significant cyclic stress. For this reason, procedures for preparing the portion of the test specimen, on which the calculated fatigue stresses are imposed, require standardization to permit correlation of results from different sources. Preparation begins with centering and rough machining. The specimen is then finished with a sharp tool and light cuts to prevent bending, overheating or cold working. The final step is a polishing operation to remove the scratches caused by machining or grinding. Generally, any method which produces a smooth surface without cold working, imposing residual stresses, or altering the material structure is considered good polishing.[7]

In fatigue testing, nearly every parameter involved is subject to some degree of variability. The significance of loading accuracy can be appreciated by realizing the relationship between loading level and fatigue life. For example, a 5% error in load amplitude can result in almost a 40% error in fatigue life. For this reason, fatigue testing tends to be conducted within horizontal bands centered at the "nominal" stress level.

The probit method is one method of statistically defining the fatigue strength of a material. Applied to fatigue testing, this technique involves evaluating a group of specimens at several uniformly spaced stress levels. A selected stress level, a certain number of stress cycles will result in specimen failure, or the prescribed cycle limit will be reached prior to failure and the sample will "runout". For this study, the prescribed cycle limit was considered to be 10^7 cycles. The percentage of specimens that will fail after a specific number of cycles for a particular material will increase as the severity of the stress or strain cycle increases. The advantage of the probit test procedure is that it can be used to develop accurate estimates of the survival percentage at point away from the median stress level on the response curve. However, this requires testing of approximately 50 samples to develop a response curve to the 5% and 95% survival limits.

Due to the fact that only 20 to 30 samples of each material/condition were available, and the primary goal was to estimate the median fatigue endurance limit (50% FEL), the staircase method was used for this analysis. The staircase method is simply an abbreviated form of the probit method. The staircase method of testing for this analysis was regulated so that there were both failures and "runouts" at a minimum of two stress levels. Statistical analysis of staircase data is a straightforward method for producing estimates of the mean fatigue strength at a specific fatigue-life value.

      1) Calculate the percentage of failures for each stress level
      2) Plot these percentages on log-normal paper with the corresponding stress levels
      3) A linear relationship is assumed, so a line was drawn connecting the data points

From the plots, the fatigue endurance limit (FEL) at 50% and 90% was determined. (extrapolation was used to estimate 90% FEL). The 50% FEL represents the stress level where 50% of the specimens will break and 50% will "runout". The 90% FEL represents the stress level where 90% of the specimens will "runout" and 10% will break. For this study, 90% FEL values were calculated for informational purposes only.[8]

Axial fatigue testing, which was not conducted for this study, requires large testing forces and rugged machine construction. The specimen is subjected to uniform stresses throughout the cross section but perfect axial loading is difficult to obtain under normal test conditions. For the same size specimens, axial load systems must be capable of applying greater forces than bending machines to achieve the same maximum stress levels. Previous work by Sanderow ("Fatigue Properties of P/M Materials: Relationship to RBF and AF Results to Material-Processing Parameters") has shown that there is a clear correlation factor between the two test methods - in general:

Axial Fatigue = 1.5 + (0.84) Rotating Bending Fatigue

The only materials that appear to deviate from this relationship are diffusion alloyed P/M steels.[9]

Microstructural Analysis

Metallographic specimens of all test materials were analyzed in the unetched as well as etched conditions. Unetched metallographic samples were utilized to evaluate stereological parameters of the pore structure such as pore shape, pore size and pore spacing. This was accomplished with a Clemex 1024C automated image analysis system, and the data analysis was based upon techniques established by DeHoff and Aigeltinger.[10]

Analysis of the pore shape was conducted to determine the average degree of circularity and distribution of the pores present in the structure. Circularity is determined by a form factor:

$$\textbf{Form Factor} = 4\,\Pi\,A\,/\,(P)^2$$

where

       A = Area of pore
       P = Circumference of pore in plane of analysis

A form factor of 1 represents a circular pore in the plane of analysis and as the number decreases from 1, the degree of irregularity increases. The form factor can predict the degree of irregularity, but not symmetry.   Form factors of some typical shapes can be seen in Figure 2.

Etched samples were examined utilizing optical microscopy to evaluate the microstructural constituents present in the material as well as to examine the crack propagation of the fatigue samples.
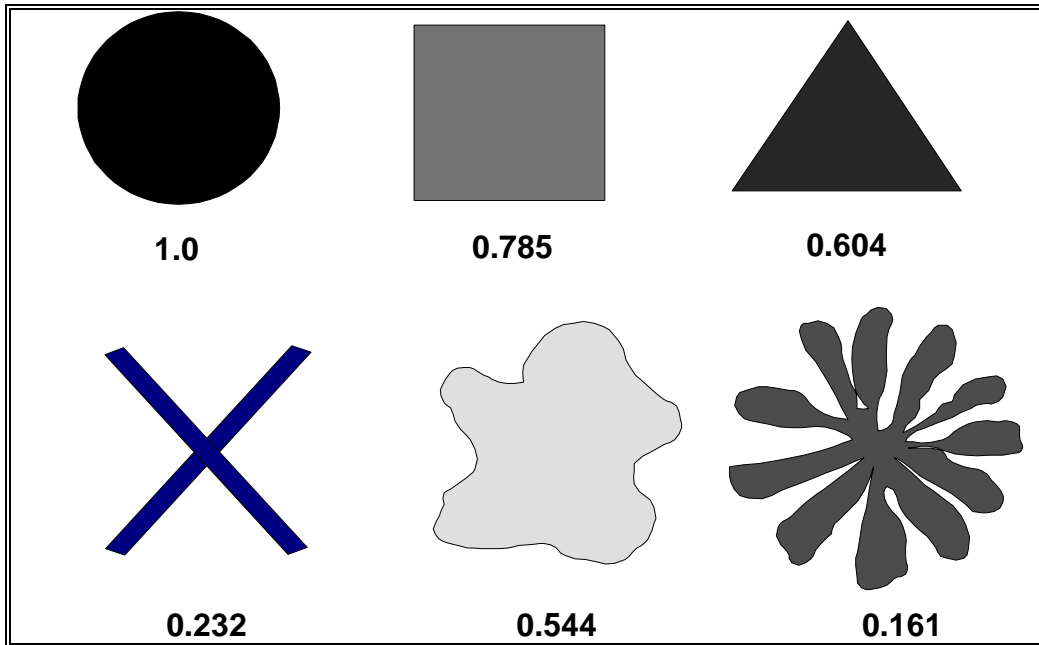
Figure 2: **Form Factors for some typical shapes**

RESULTS

The tensile and fatigue properties for all test materials are summarized in Table III, as well as the 50% FEL as a percentage of the ultimate tensile strength at sintering temperatures of 2050°F (1120°C) and 2300°F (1260°C). Due to the variability between the specimen types, the density of the tensile specimens did not exactly match that of the fatigue specimens. To correlate the data, tensile properties were interpolated from available data.

Table III: Fatigue and Tensile Properties for FLN2-4405 Premixes Sintered at 2050°F (1120°C) / 2300°F (1260°C)

Material	Sintering Temperature (°F / °C)	Density (g/cm³)	UTS (10³ psi / MPa)	50% FEL (10³ psi / MPa)	90% FEL (10³ psi / MPa)	50% FEL as % UTS
Mix A		6.88	59.0 / 407	23.4 / 161	22.5 / 155	39.7
		7.05	67.0 / 462	27.5 / 189	24.5 / 169	41.0
		7.27	74.0 / 510	31.8 / 219	31.6 / 218	43.0
Mix B	2050 / 1120	6.89	64.0 / 441	26.3 / 181	25.2 / 174	41.1
		7.06	78.0 / 537	30.5 / 210	27.3 / 188	39.1
		7.27	92.0 / 634	35.4 / 244	33.8 / 233	38.5
Mix C		7.07	71.0 / 490	29.9 / 208	28.7 / 198	42.1
		7.34	83.2 / 574	31.8 / 219	28.6 / 197	38.2
Mix D		7.15	88.5 / 610	31.9 / 220	29.4 / 203	36.0
		7.32	95.1 / 656	35.4 / 244	33.9 / 234	37.2
Mix A		6.92	82.0 / 565	25.5 / 176	23.0 / 159	31.1
		7.11	87.5 / 603	28.6 / 197	26.1 / 180	32.7
		7.26	92.5 / 637	33.7 / 232	28.9 / 199	36.4
Mix B	2300 / 1260	6.93	73.5 / 506	25.9 / 178	23.2 / 160	32.6
		7.11	84.0 / 579	30.1 / 207	29.0 / 200	32.6
		7.27	92.5 / 637	36.0 / 248	34.3 / 236	36.0
Mix C		7.12	87.2 / 601	29.5 / 203	27.0 / 186	33.8
		7.38	102.0 / 703	34.9 / 240	32.0 / 221	34.2
Mix D		7.21	93.8 / 647	33.0 / 227	31.5 / 217	35.2
		7.35	100.6 / 694	35.3 / 243	34.0 / 234	35.1

Mean pore spacing and average pore size values are summarized in Table IV. Stereological data for pore shape and cumulative percent pore size of the materials was not put into tabular form due to the fact that the amount of data was too substantial. These results are summarized in graphical form in the discussion section.

DISCUSSION

Sintered Density / Sintering Temperature

Sintered density versus UTS, at sintering temperatures of 2050°F (1120°C) and 2300°F (1260°C), is plotted for Mixes A and C in Figure 3, and Mixes B and D in Figure 4. The two primary variables examined were nickel particle size and processing method.

In regard to the nickel particle size, Figure 3 shows the relationship for Mixes A and C, which contain coarse nickel. At a temperature of 2050° F, the sintered density increases linearly with UTS. As the temperature is increased to 2300°F (1260°C), a linear relationship still exists, but the UTS at a given density level increases a minimum of 19 % - 20%. This is most likely due to a higher degree of microstructural homogenization with increasing sintering temperature.

Figure 4 shows the relationship for Mixes B and D, which contain standard grade nickel. At a temperature of 2050° F, the sintered density increases linearly with UTS. An increase in the sintering temperature to 2300°F (1260°C), does not alter the relationship. So, the UTS at a given density level appears constant and independent of temperature.

In regard to processing method, the plots indicate that over comparable density ranges the relationship between sintered density and UTS appears comparable for conventional and ANCORDENSE processed materials. So, in general, the relationship between sintered density and UTS does not appear to be affected by processing method. The only variable that appears to affect this relationship is nickel particle size.

Table IV: Stereological Data

Material	Sintering Temperature (°F) / (°C)	Density (g/cm³)	Average Pore Size (um)	Mean Pore Spacing (µm)
A		6.88	102	34.7
		7.05	80	40.4
		7.27	59	54.5
B	2050 / (1120)	6.89	104	38.5
		7.06	75	45.3
		7.27	58	50.1
C		7.07	83	44.7
		7.34	50	50.1
D		7.21	67	45.9
		7.35	50	50.7
A		6.92	98	44.9
		7.11	82	47.5
		7.26	54	45.7
B	2300 / (1260)	6.93	110	43.8
		7.11	80	48.8
		7.27	54	60.5
C		7.12	93	49.0
		7.38	52	73.4
D		7.15	83	52.1
		7.32	58	60.1

Ultimate Tensile Strength

The relationship between ultimate tensile strength and 50% FEL at sintering temperatures of 2050°F (1120°C) and 2300°F (1260°C) for Mixes A through D is shown in Figures 5 and 6. The 50% FEL value was utilized because it has the highest degree of accuracy. The staircase method dictates that the degree in validity of the fatigue endurance value decreases as you deviate from the mean value.

For each individual material and sintering temperature, the improvement in strength realized by higher density of a given material is indicated as an increase in 50% FEL. However, the data clearly indicates that fatigue endurance limit is not solely a function of the UTS. Two important points:
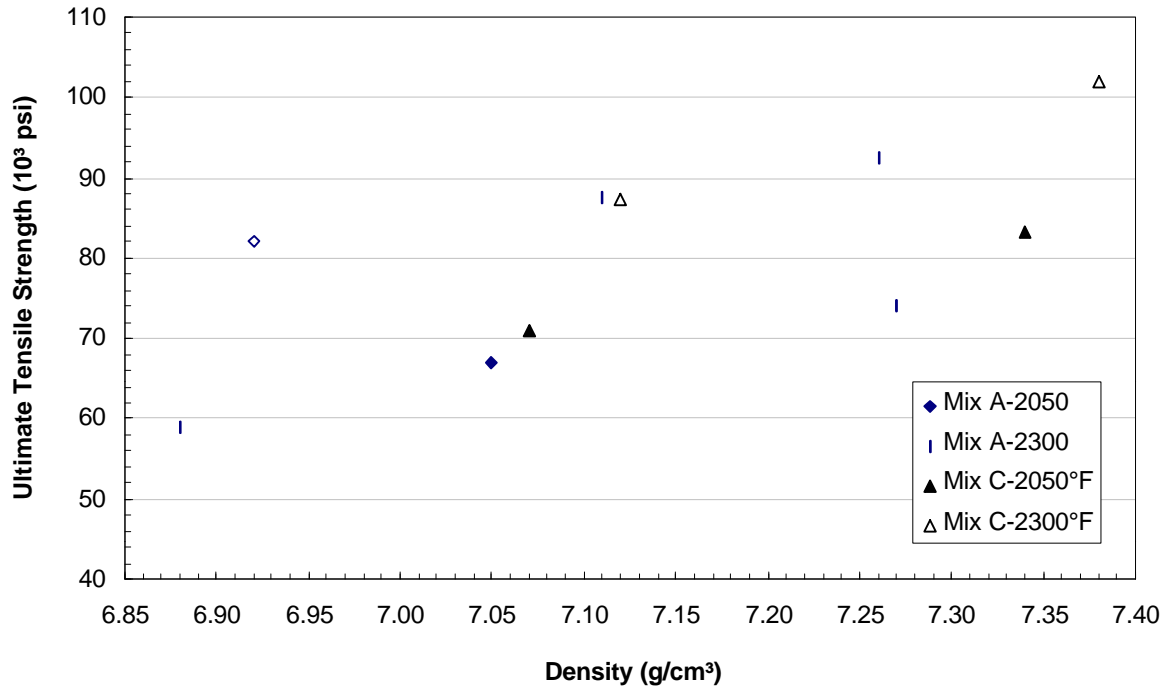
Figure 3: Density versus UTS - Materials containing (~50µm Nickel)
Sintering Temperatures 2050°F (1120°C) / 2300°F (1260°C)
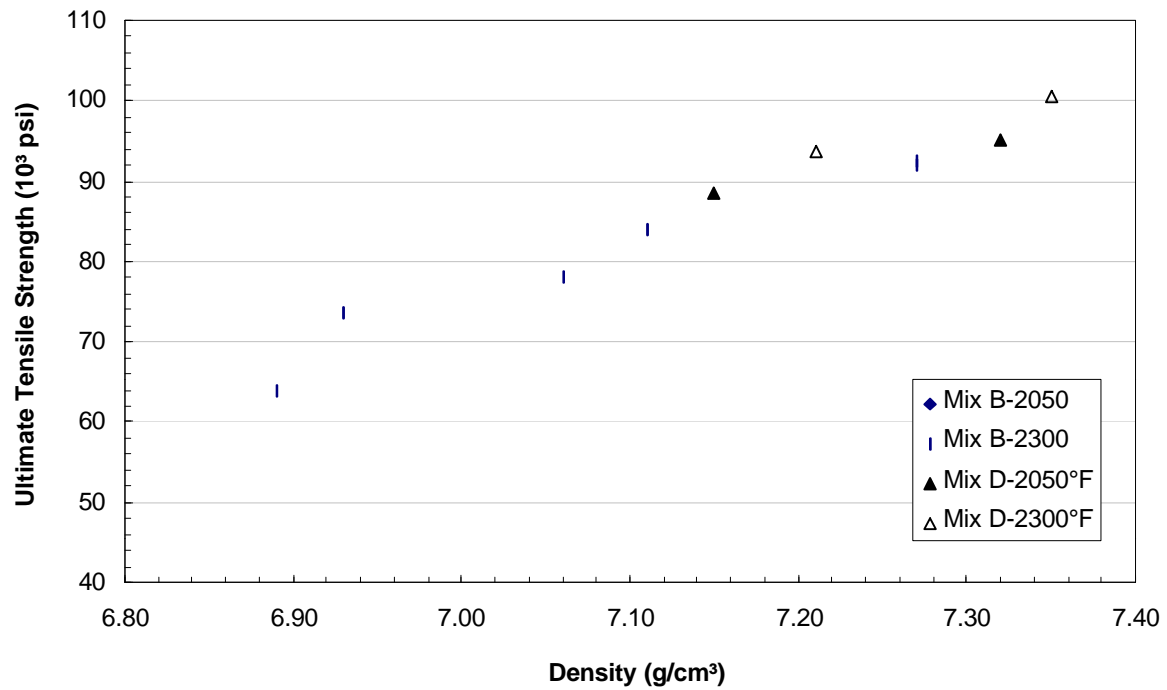
Figure 3: Density versus UTS - Materials containing (~4µm Nickel)
Sintering Temperatures 2050°F (1120°C) / 2300°F (1260°C)

- At lower density levels, the effect of nickel is apparent. At comparable sintered density values, Mixes A and C show lower UTS and 50% FEL values at a given density level than Mixes B and D. Increasing the sintering temperature results in an increase in sintered density and UTS for all materials without a significant corresponding increase in 50% FEL

- At higher density levels the effect of nickel is still present. At a sintering temperature of 2050°F (1120°C) and comparable sintered density values, Mixes A and C show lower UTS and 50% FEL at a given density level values than Mixes B and D. Increasing the sintering temperature does not substaintially increase the sintered density of any the materials. However, for Mixes A and C, increasing the temperature increases the UTS and 50% FEL to be comparable to that of Mixes B and D

- At the highest density levels and sintering temperatures, there is a correlation between UTS, 50% FEL and sintered density that is comparable for all materials examined

Fatigue Ratio

Figures 7 and 8 highlight 50% FEL as a percentage of UTS for Mixes A through D, at density levels of 7.0 g/cm³ and 7.2 g/cm³, and sintering temperatures of 2050°F (1120°C) and 2300°F (1260°C). This value is commonly referred to as the "fatigue ratio" To aid data analysis, the fatigue ratios for all materials and conditions were superimposed onto plots 7 and 8. For many years, the fatigue ratio was considered to be a constant percentage of the UTS for all P/M materials. However, recent research has shown that this clearly is not the case.[1,2,3,8] Although the data does correlate with previous work that showed the fatigue ratio increased with increasing nickel particle size at low density levels and sintering temperatures, this study examined the effects of sintering temperature and density level in more detail. The interesting trend that is worth noting is the correlation between the fatigue ratios of the materials and the UTS versus 50% FEL relationships, which appear to hold true for both the conventional and ANCORDENSE processed materials. For example, the fatigue ratio for Mixes A, B and C, at lower density levels and a sintering temperature 2050°F (1120°C), varies between 39% to 42%. As the sintering temperature is increased to 2300°F (1260°C), the fatigue ratio for all mixes varied between 33% and 34%. This is a decrease of approximately 18%. Mix D did not correlate with the other materials at the lower density levels. The probable explanation is the fact that Mix D had a sintered density value approximately 0.10 g/cm³ higher than that of Mix C.
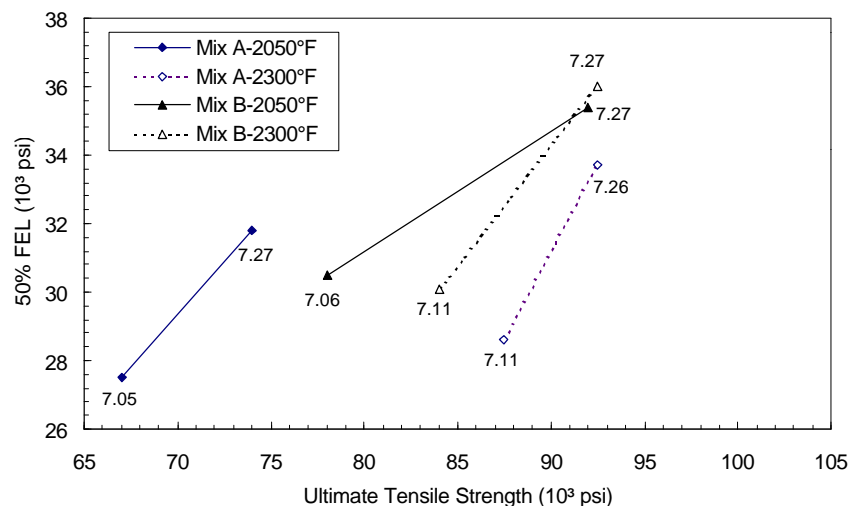
Figure 5:   Ultimate Tensile Strength versus 50% FEL - Conventional Materials Sintering Temperatures 2050°F (1120°C) / 2300°F (1260°C)
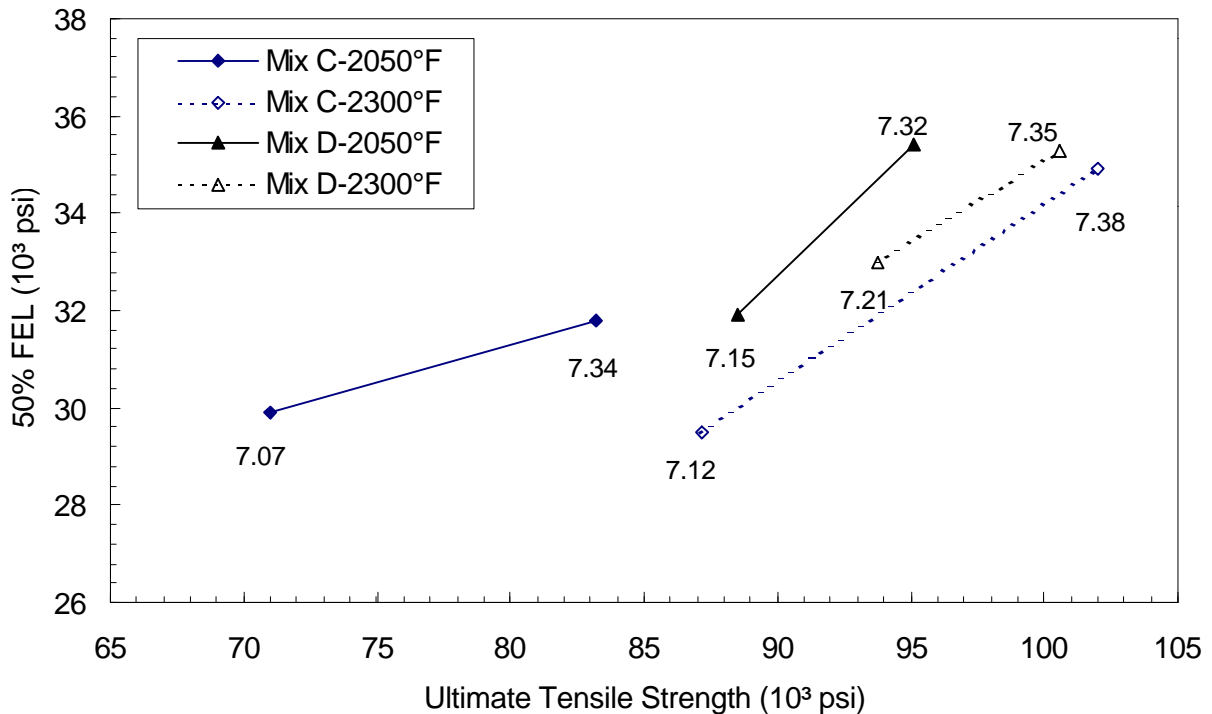
Figure 6: **Ultimate Tensile Strength versus 50% FEL - Conventional Materials Sintering Temperatures 2050°F (1120°C) / 2300°F (1260°C)**

At the higher density levels, the fatigue ratio for Mixes A and C, varies between 38% and 43%, and the fatigue ratio of Mixes B and D is 37%, at a sintering temperature of 2050°F (1120°C). As the sintering temperature increased to 2300°F (1260°C), the fatigue ratios of materials A through D become fairly comparable, varying between 34% and 36%. This is a decrease of 13% for Mixes A and C, and only 4% for Mixes B and D.

The results seem to indicate that at lower density levels, the fatigue ratio was generally consistent for all test materials, independent of processing method or type of nickel. However, the fatigue ratio does decrease with increasing sintering temperature. A similar trend is seen at the higher density levels, the only difference being that, Mixes B and D show a slightly lower fatigue ratio at 2050°F (1120°C) compared with that of Mixes A and C.

Work by Sanderow states that the strongest variable that influences the fatigue ratio is the material microstructure. He states the following:

"Fatigue Ratio = 39% (ferrite + pearlite) microstructures for carbon content (0.5%-0.8%)
Fatigue Ratio = 32% martensitic microstructures" [9]

The microstructure of the materials is examined in more detail in the next section to determine if the relationship between sintering temperature and fatigue ratio can be attributed to pore structure or the homogenization of the microstructure with increasing temperature.

Stereological Parameters

Stereological parameters, including pore shape, cumulative percent pore size, mean pore spacing and average pore size were examined to evaluate the effects of pore structure on fatigue properties.

Plots of pore shape at 2050°F (1120°C) and 2300°F (1260°F) for Mixes A through D compacted to a green densities of 7.0 g/cm³ and 7.2 g/cm³ are shown in Figures 9 and 10.   As expected, with increasing sintering temperature the pore shape of all the materials that were evaluated became more circular. There appears to be no significant change in the pore shape as the density is increased from 7.0 g/cm³ to 7.2 g/cm³. The behavior of the materials indicates that the nickel particle size, processing method and material density have very little effect on the pore shape of the test materials, which correlates with previous work that was conducted.[3]
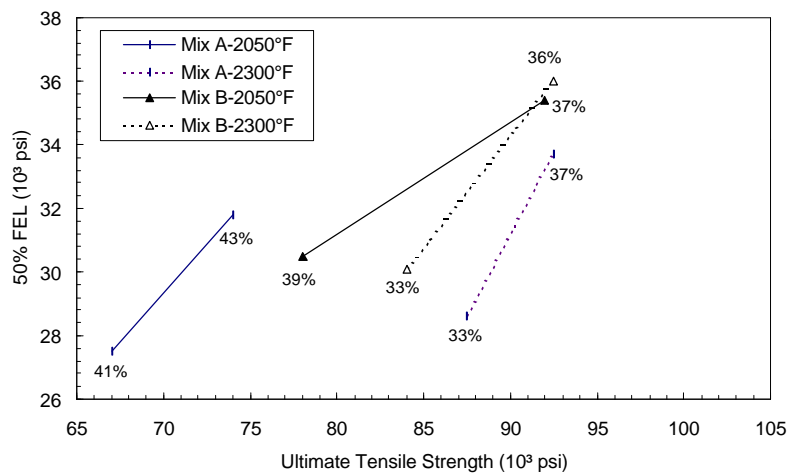
**Figure 7:   Fatigue Ratios - Conventional Materials
        Sintering Temperatures 2050 °F (1120°C) / 2300°F (1260°C)**
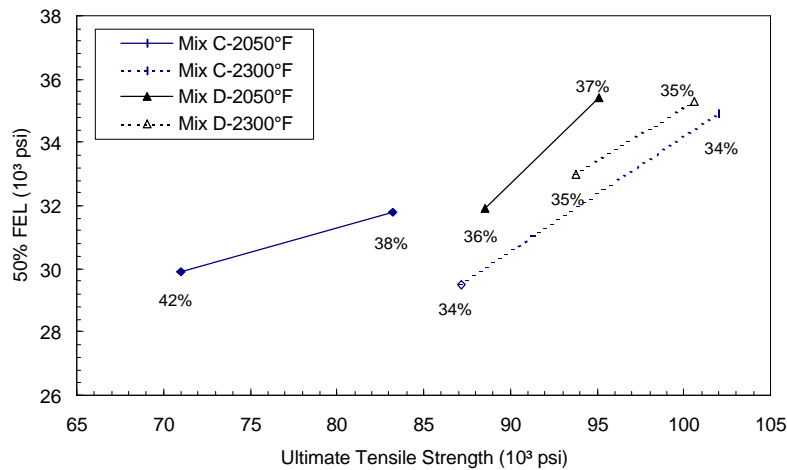
Figure 8 -   Fatigue Ratios - ANCORDENSE Materials

Sintering Temperatures 2050°F (1120°C) / 2300°F (1260°C)
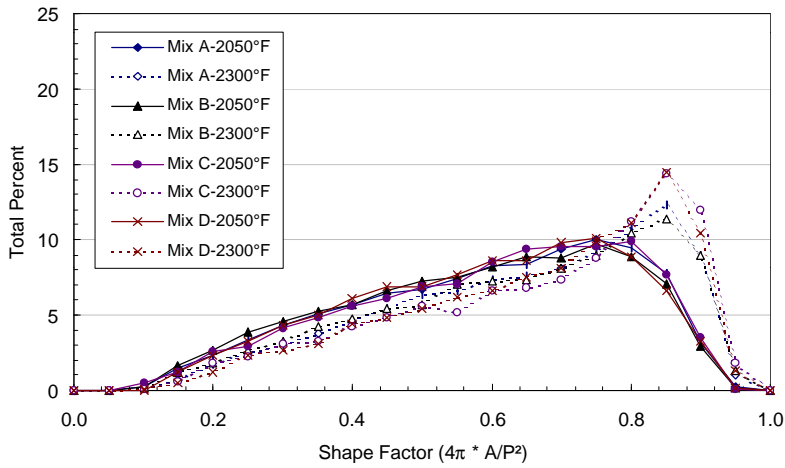
Figure 9: **Pore Shape of FN-0205 Premixes - Compacted to Green Density - 7.0 g/cm³**
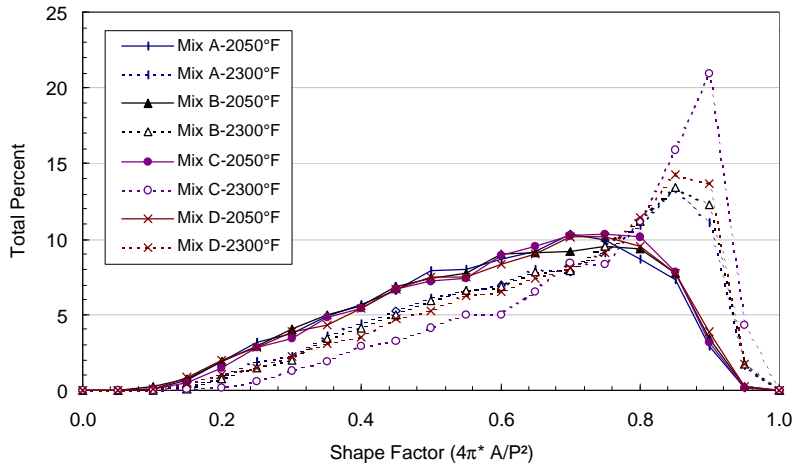
Figure 10: **Pore Shape of FN-0205 Premixes - Compacted to Green Density - 7.2 g/cm³**

Plots showing the cumulative percent pores versus pore size less than a given a size at 2050°F (1120°C) and 2300°F (1260°C) for Mixes A through D compacted to green densities of 7.0 g/cm³ and 7.2 g/cm³ are shown in Figures 11 & 12. As expected, the pore structure becomes finer with increasing sintered density and coarser with increasing sintering temperature, with the effect of density being the more pronounced variable. Although the plots show variations in pore structure, there are no characteristics that would explain the different fatigue response at density levels of 7.0 g/cm³ and 7.2 g/cm³, which correlates with previous work that was conducted.

The mean pore spacing versus the 50% FEL, at density levels of 7.0 g/cm³ and 7.2 g/cm³ and sintering temperatures of 2050°F (1120°C) and 2300°F (12060°C), is plotted in Figures 13 Figure 14. Figure 13, which highlights the trends at 7.0 g/cm³, clearly shows a relationship between mean pore spacing and 50% FEL - as the mean pore spacing increased, the 50% FEL increased. Although increasing the sintering temperature does increase the mean pore spacing

for a given value of 50% FEL, the relationship is clearly still strong. The trend lines that were inserted into the plot show correlation factors of 81% at 2050°F (1120°C) and 95% at 2300°F (1260°C). Previous studies have shown some degree of correlation between mean pore spacing and 50% FEL. However, this correlation is significantly increased by isolating the influence of density and sintering temperature.

Figure 14, which examines the relationship between mean pore spacing and 50% FEL at a density level of 7.2 g/cm³, does not show a relationship between these two variables. The trend lines that were inserted in the plot show correlation factors of 27% at 2050°F (1120°C) and 29% at 2300°F (1260°C). This seems to indicate that mean pore spacing is an important variable in predicted 50%FEL at lower density levels while its importance apparently decreases as the density level is increased.

Figures 15 shows the average pore size of the conventionally processed materials superimposed onto the data points of plots 5 and 6, which show the relationship of UTS versus 50% FEL. The plot shows that the average pore size at lower density levels varies between
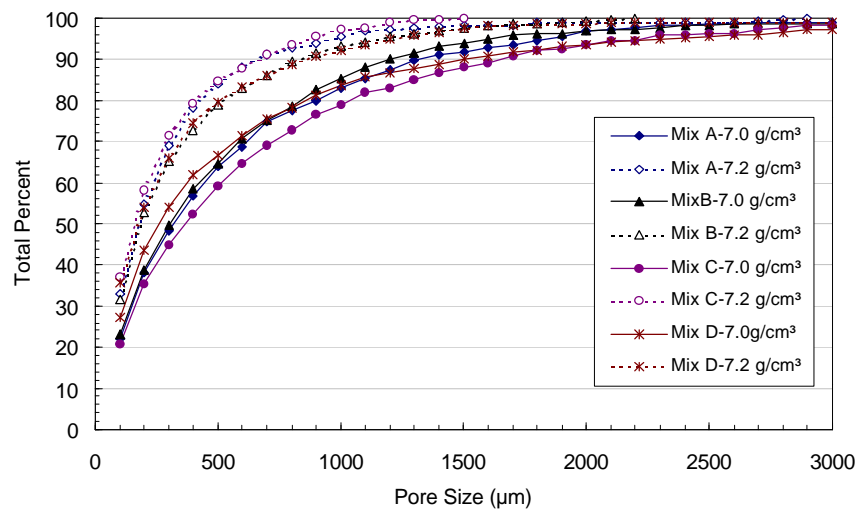
Figure 11:   Pore Size versus Cumulative Total % - Sintering Temperature 2050°F
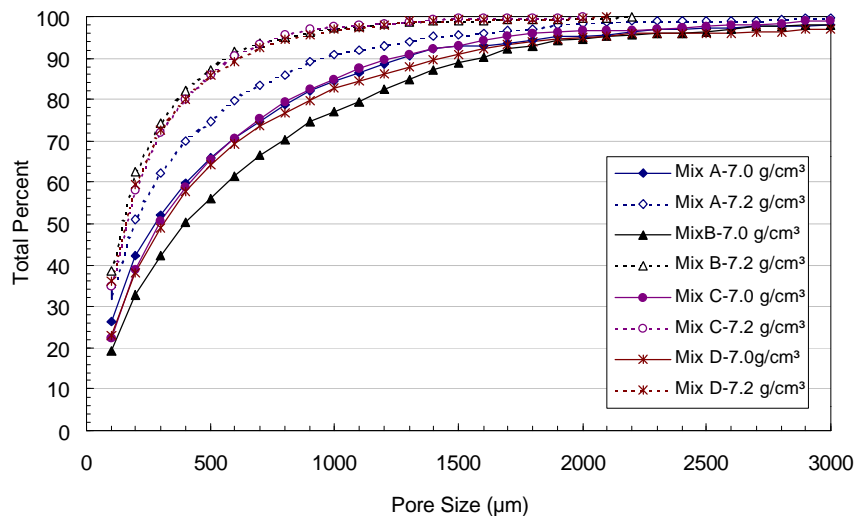
Figure 12:   Pore Size versus Cumulative Total % - Sintering Temperature 2300°F

75 and 80 µm, with the correlating sample density varying between 7.05 g/cm³ and 7.11 g/cm³. Although these values of average pore size and density are fairly consistent for both Mixes A and B, they correspond to a fairly significant variation in UTS of approximately 20,000 psi. As the density is increased to 7.2 g/cm³, with the exception of Mix A at 7.2 g/cm³ and 2050°F, the average pore size is 54 µm for both Mixes A and B, with a correlating sample density of 7.26 g/cm³ to 7.27g/cm³.   These values are very consistent and correspond to a variation in UTS of only 500 psi.

Overall, at higher density levels it appears that the UTS, sample density and average pore size correlate. At lower density values, there is a correlation only between the sample density and average pore size.

The trends that were seen for the conventional materials also held true for the ANCORDENSE processed materials. It is also interesting to note that the overall average pore size at the higher density levels for the ANCORDENSE and conventional materials was 53 µm and 54 µm respectively. So, at these higher density levels all the test materials show the same average pore size, independent of sintering temperature, nickel type or processing method. This seems to indicate that average pore size is a variable that influences the fatigue properties.

Additional work needs to be done to adequately explain the behavior of Mixes A and C at 7.2 g/cm³ and 2050°F (1120°C).

Microstructure

Photomicrographs of the etched structures are shown in Figures 16 and 17. Figure 16 shows Mixes A through D at a density level of 7.0 g/cm³ and a sintering temperature of 2050°F (1120°C). Figure 17 shows Mixes A through D at a density level of 7.2 g/cm³ and a sintering temperature of 2300°F (1120°C). These micrographs were chosen for discussion because, as previously discussed, at a density level of 7.0 g/cm³ and sintering temperature of 2050°F (1120°C), for both types of nickel and processing methods that were utilized for this study there is no clear correlation between UTS and 50% FEL. As the density level and sintering temperature increased to 7.2 g/cm³ and 2300°F (1260°C), all the materials appear to show similar behavior; the relationship between UTS and 50% FEL is consistent and does not appear to be affected by nickel type or processing method. These conditions also are critical in regard to the stereological parameters.

Examining the photomicrographs in Figure 16 shows that the microstructure of all four mixes is primarily divorced pearlite with small areas of bainite or partially transformed martensite. However the bainitic or martensitic areas were more numerous in Mixes B and D. This is most likely due to the higher degree of microstructural homogenization of these materials. The microstructures of all four materials contain nickel rich regions, and visually examining the entire area of the samples revealed that the largest nickel regions were visible in Mixes A and C. Mixes A through D show similar pore structures, with all samples clearly showing some areas of larger porosity.

The photomicrographs in Figure 17 show a general coarsening of the pearlite with increasing sintering temperature as well as a higher percentage of martensitic/bainitic areas. As with the samples in Figure 16, the highest degree of microstructural homogenization is seen with Mixes B and D, while nickel rich areas are still clearly visible in Mixes A and C. There are changes in the pore structure of all the materials due to higher sintering temperature and increased

density. The overall pore structure is finer and there also do not appear to be any very large pores present comparable to what was seen at the lower density levels.
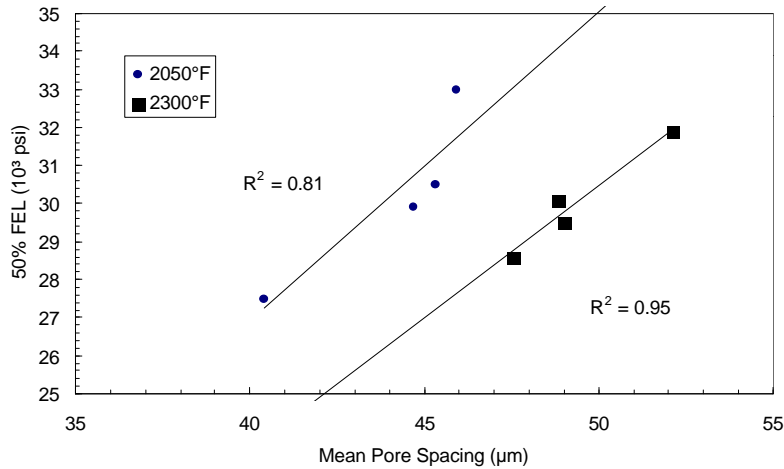
Figure 13:   Mean Pore Spacing versus 50% FEL - Green Density 7.0 g/cm³
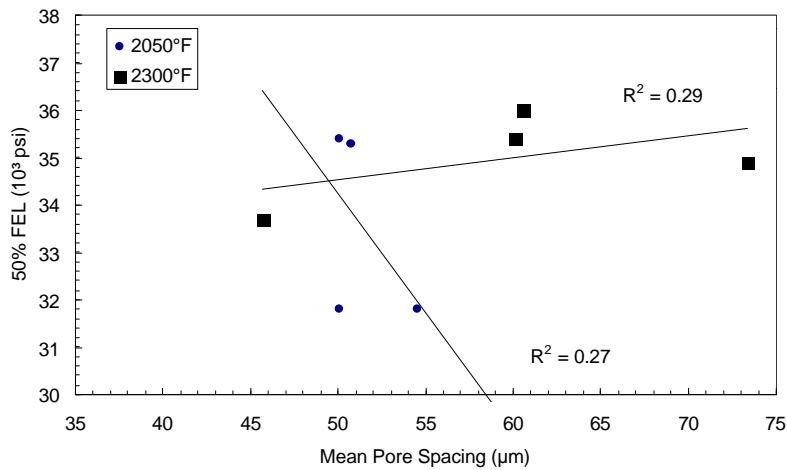
Figure 14:   Mean Pore Spacing versus 50% FEL - Green Density 7.2 g/cm
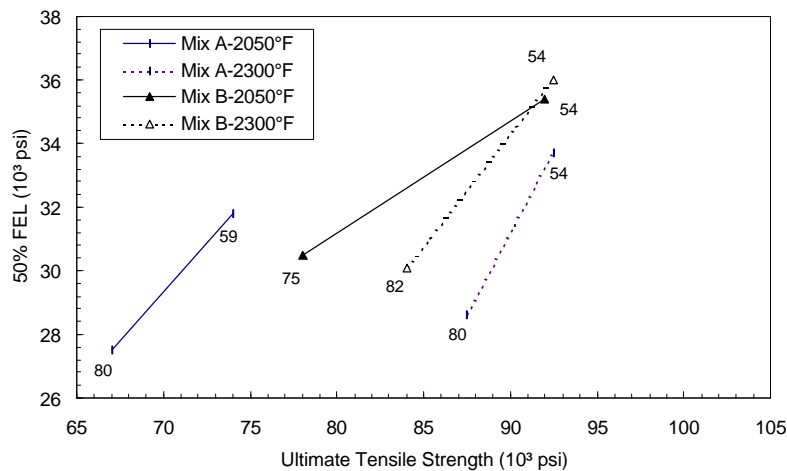
Figure 15:   Average Pore Size - Conventional Materials

Although photographing the fatigue crack propagation path was attempted for all materials, it was only successful for 6 out of the 8 samples. For the lower density samples, the crack propagation clearly favors areas of porosity, primarily the very large pores (Figure 17 B and C). As the density is increased, the crack does not favor areas of porosity and appears to travel along the grain boundaries (Figure 18 B and C). This seems to support the influence of stereological parameters upon fatigue properties at lower density levels that was seen in this study.

This continuing study of fatigue properties in P/M materials provides more evidence for the fact that the fatigue endurance limit of a material is a complex relationship between many factors. The findings indicate that up to a certain critical sintered density level, in this case approximately 7.1 g/cm, the morphology of the pore structure does influence the fatigue properties of P/M materials. As the density level is increased, and the average pore size and spacing decreases to certain level, this influence of stereological parameteres decreases and the fatigue properties become primarily a function of microstructure.

CONCLUSIONS

1. Although the analyzed density ranges were comparable for both the conventional and ANCORDENSE processed materials, the effect of density upon UTS does not appear to be affected by the processing method. However, it does appear to be affected by admixed nickel particle size.

2. At lower density levels, the effect of nickel is apparent. At comparable sintered density values, Mixes A and C show lower UTS and 50% FEL values at a given density level than Mixes B and D. Increasing the sintering temperature results in an increase in sintered density and UTS for all materials without a significant corresponding increase in 50% FEL

3. At higher density levels the effect of nickel is still present. At a sintering temperature of 2050°F (1120°C) and comparable sintered density values, Mixes A and C show lower UTS and 50% FEL values at a given density level than Mixes B and D. Increasing the sintering temperature does not substaintially increase the sintered density of any the materials. However, for Mixes A and C, increasing the temperature increases the UTS and 50% FEL to be comparable to that of Mixes B and D

4. At higher density levels, Mixes A and C show a 13% decrease in the fatigue ratio with increasing sintering temperature. For Mixes B and D, the fatigue ratio was lower than what was seen for Mixes A and C at 2050°F, and showed only a 4% decrease as the sintering temperature increased to 2300°F (1260°C).

5. The nickel particle size, processing method and material density had very little effect on the pore shape of the test materials, which correlates with previous work that has been conducted.

6. As expected, the pore structure becomes finer with increasing sintered density and coarser with increasing sintering temperature, with the effect of density being the most pronounced variable. However, there are no characteristics in the pore size analysis that would explain the different fatigue response at density levels of 7.0 g/cm³ and 7.2 g/cm³.

7. At a density level of 7.0 g/cm³, there appears to be a relationship between mean pore spacing and 50% FEL - as the mean pore spacing increased, the 50% FEL increased. At

a density level of 7.2 g/cm³, there did not appear to be a relationship between these two variables. Previous studies have shown some relationship between mean pore spacing and 50% FEL. However, the correlation is significantly increased by isolating the influence of density and temperature.

8. At higher density levels it appears that the UTS, sample density and average pore size correlate. At lower density values there is a correlation only between the sample density and average pore size.

9. For the lower density samples, the crack propagation clearly favors areas of porosity. As the density is increased, the crack propagation does not favor areas of porosity and appears to travel along the grain boundaries.
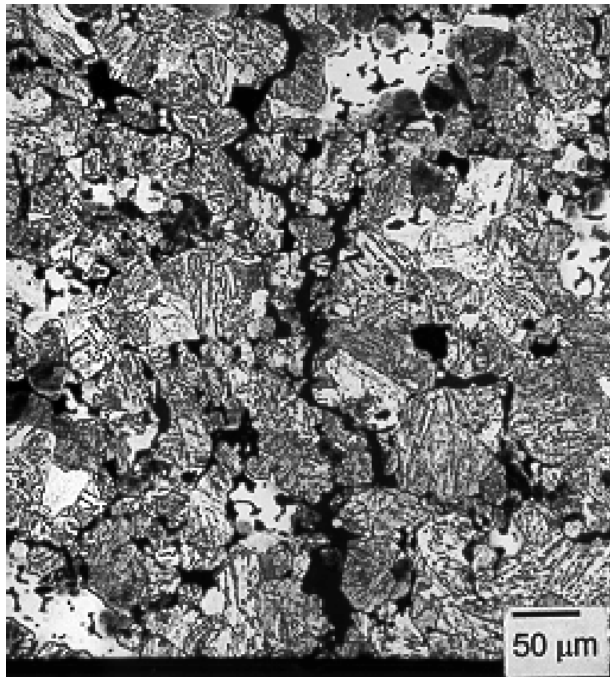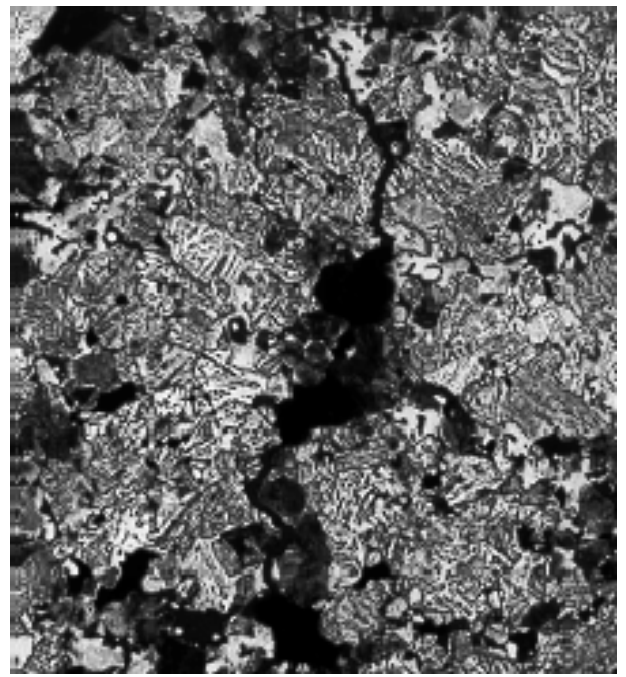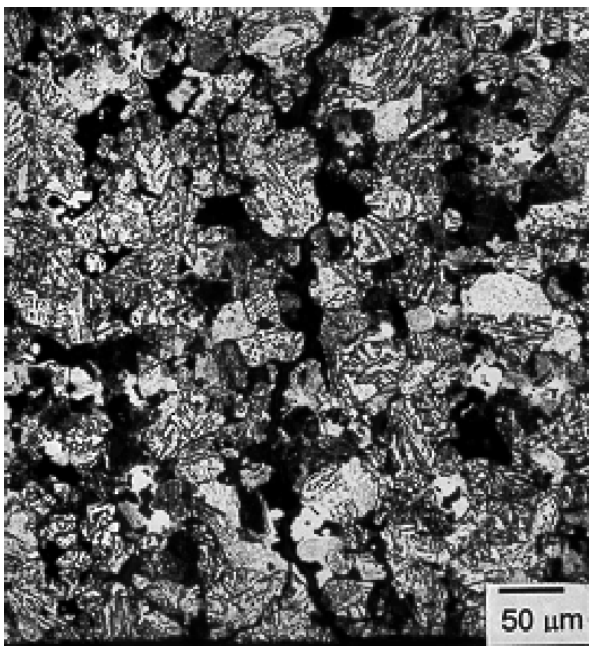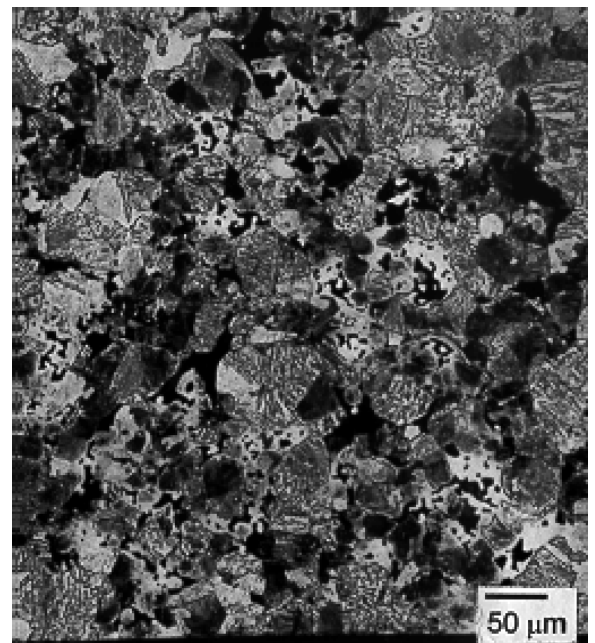
Mix A

Mix B

Mix C

Mix D

Figure 17: **Photomicrographs of Etched Microstructures - Green Density - 7.0 g/cm³ Sintering Temperatures 2050°F (1120°C)**
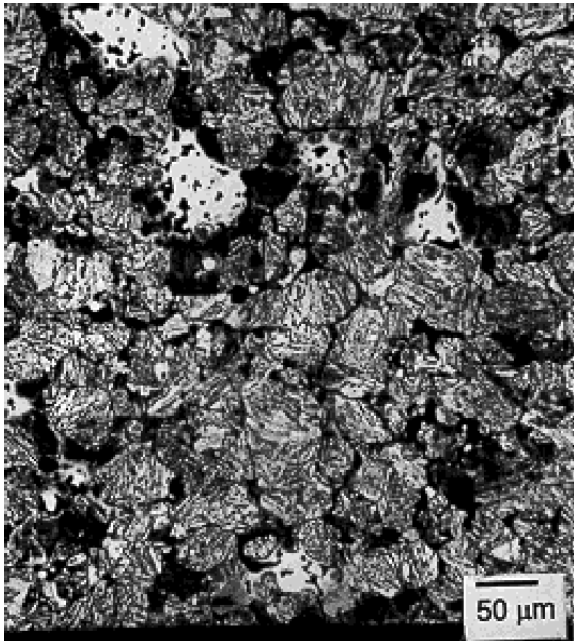
Mix A
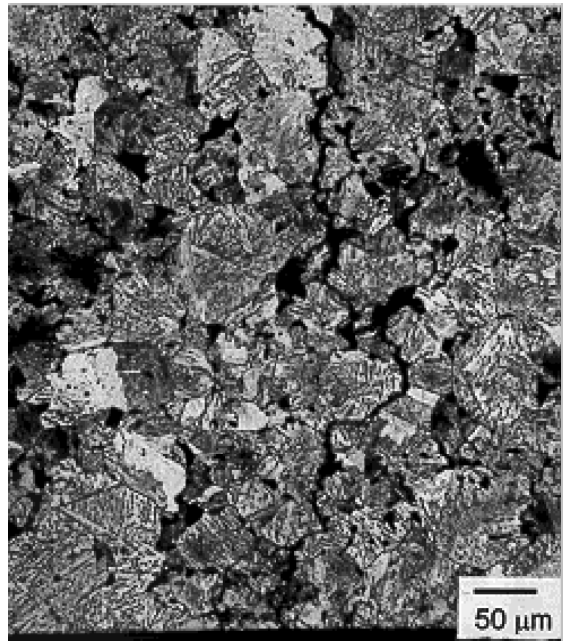
Mix B
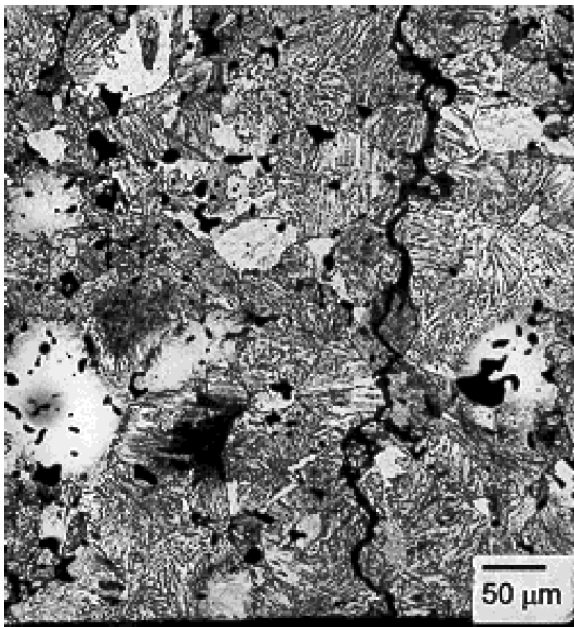
Mix C
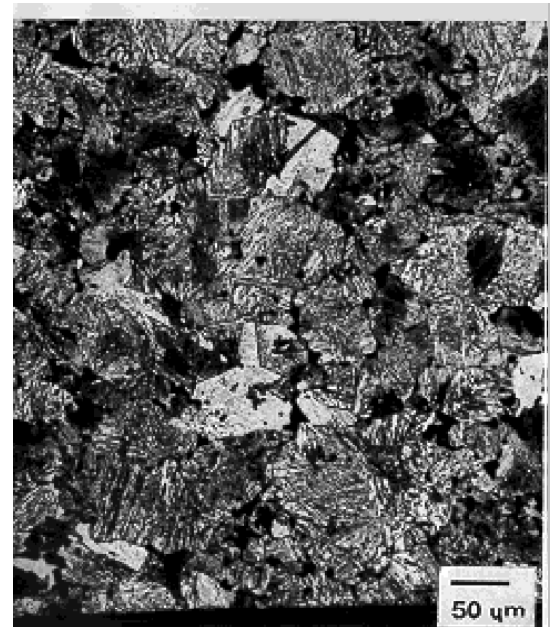
Mix D

Figure 18: **Photomicrographs of Etched Microstructures - Green Density - 7.2 g/cm³ Sintering Temperatures 2300°F (1120°C)**

REFERENCES

1. Rutz, H.G., Murphy, T.F., Cimino, T.M., "The Effect of Microstructure on Fatigue Properties of High Density Ferrous Materials", *Advances in Powder Metallurgy and Particulate Materials-1996*, Vol. 4, pp 13-375 13-389, Metal Powder Industries Federation, Princeton, NJ.

2. Cimino, T.M., Rutz, H.G., Murphy, T.F., Graham, A.H.,"The Effect of Microstructure on Fatigue Properties of Ferrous P/M Materials", *Advances in Powder Metallurgy and Particulate Materials-1997*, Vol. 2, pp 13-137 13-149, Metal Powder Industries Federation, Princeton, NJ.

3. Cimino, T.M., Graham, A.H., Murphy, T.F.,"The Effect of Microstructure and Pore Morphology on Mechanical and Dynamic Properties of Ferrous P/M Materials", *Advances in Powder Metallurgy and Pariculate Materials-1998*, Vol x, pp   , Metal Powder Industries Federation, Princeton, NJ

4. Rutz, H.G., Hanejko, F.G., "High Density Processing of High Performance Ferrous Materials", *Advances in Powder Metallurgy and Pariculate Materials-1994*, Vol. 5, pp. 117-133, Metal Powder Industries Federation, Princeton, NJ.

5. "Standard Test Methods for Metal Powders and Powder Metallurgy Products", Metal Industries Federation, Princeton, NJ, 1998.

6. "Manual on Fatigue Testing", University Microfilms, Inc., Baltimore, MD, 1949.

7. "Handbook of Fatigue Testing", American Society for Testing and Materials, Baltimore, MD, 1974.

8. Sanderow, H.I., Spirko, J.R., Freidhoff, T.G., "Fatigue Propeties of RBF and AF Results of Material-Processing Parameters", *Advances in Powder Metallurgy and Particulate Materials-1997*, Vol. 13, pp 117-136, Metal Powder Industries Federation, Princeton, NJ.

9. DeHoff, R.T., Aigeltinger, E.H., "Experimental Quantitative Microscopy with Special Applications to Sintering", Perspectives in Powder Metallurgy--Volume 5--Advanced Experimental Techniques in Powder Metallurgy, pp81-137, Plenum Press, New York--London, 1970.